9th International Conference on
Photonic Technologies LANE 2016

# Dynamic behavior of plasma in internal modification of transparent dielectrics by USLPs

Isamu Miyamoto[a,b,*], Yasuhiro Okamoto[c], Rie Tanabe[d], Yoshiro Ito[d], Kristian Cvecek[e], Michael Schmidt[b,e,f]

[a]*OsakaUniversity, 2-1, Yamada-Oka, Suita, Osaka, 565-0877, Japan*
[b]*Erlangen Graduate School of Advanced Optical Technologies (SAOT), Paul-Gordan Str. 6, 91052 Erlangen, Germany*
[c]*Okayama University, 3-1-1 Thsushimanaka, Kita-ku, Okayama 700-8530, Japan*
[d] *Nagaoka University of Technology, 1603-1, Kamitomioka, Nagaoka, Niigata 940-2188, Japan*
[e]*Bayerisches Laserzentrum GmbH (blz), Konrad-Zuse-Straße 2-6, 91052 Erlangen, Germany*
[f]*Institute of Photonic Technologies (LPT), Friedrich-Alexander-Universität Erlangen-Nürnberg, Konrad-Zuse-Straße 3-5, 91052 Erlangen, Germany*

**Abstract**

Internal modification of bulk transparent dielectrics by ultrashort laser pulses (USLPs) has attracted much attention due to its high process performance especially at high pulse repetition rates. We previously reported high speed camera observation of plasma evolved in borosilicate glass irradiated by 550 *fs*-laser pulses at a repetition rate of 1MHz, showing the unexpected dynamic plasma behavior where high brightness plasma moves semi-periodically toward the laser source within laser-absorption region. In this paper, free-electron density evolved in internal modification of glass irradiated by USLPs at high pulse repetition rates are simulated based on rate equation model of free-electrons coupled with thermal conduction model with taking into consideration the plasma shielding effect to explain the observed dynamic plasma behavior. The simulation shows thermally ionized electrons, which contribute as the seed electrons for avalanche ionization, play an important role in ionization process to provide periodical plasma motion. It is also shown the ionized region expands toward the laser source up to the region where the laser intensity does not reach mulitiphoton ionization threshold in agreement with the experimental observation qualitatively.



*Keywords:* nonlinear absorption; avalanche ionization; seed electrons; high pulse repetition rat; dynamic plasma motion; heat accumulation

## 1. Introduction

Internal modification of transparent dielectrics by ultrashort laser pulses (USLPs) has been studied actively, since the advent of USLPs, and a variety of interesting applications have been reported including waveguide formation [1-3], fusion welding [4-6] and selective etching [7,8]. Especially internal modification at high pulse repetition rates has attracted much attention, since higher quality modification is available at higher throughput. However, much still remains to be learned about the interaction between USLPs and transparent dielectrics at high pulse repetition rates, because laser-matter interaction at high pulse repetition rates is much more complicated than that of single pulse due to heat accumulation effect.

In internal modification processes, valence electrons are promoted to conduction band by nonlinear absorption process, and then material is modified due to high density free-electrons and temperature rise. For understanding internal modification process, evolution of free-electrons has been simulated by a lot of researchers using rate equation model to account for photoionization and avalanche ionization process at different pulse durations and materials [9-12]. However, shielding effects by laser-induced plasma were mostly neglected, despite the fact that laser intensity behind the plasma is significantly reduced by the shielding effect [13].

* Corresponding author. Tel.: +81-798-47-1095; fax: +81-798-47-1095 .
*E-mail address:* miyamoto-i@ares.eonet.ne.jp

© 2016 The Authors. Published by Bayerisches Laserzentrum GmbH

Temperature rise also plays an important role in ionization process at high pulse repetition rates making the process understanding difficult, since absorbed laser energy is transferred to the lattice to produce very high temperature rise. At low pulse repetition rates, the temperature rise is suppressed by the thermal diffusion between laser pulses, and hence the effect of temperature rise on absorption process can be neglected. At high pulse repetition rates, however, the absorption process becomes complicated due to heat accumulation effect, since the absorption process is significantly affected by temperature rise.

The contribution of heat accumulation in internal modification was first reported by Schaffer *et al* [14]. They reported that bulk glass can be internally melted at pulse energy as low as 5 *nJ* at a repetition rate of 25 *MHz* while no internal melting occurs with single pulse irradiation, and that the dimension of the molten region increases as the pulse number increases in agreement with experimental observation. However, the simulated melt dimension agrees with experimental values only at smaller pulse number where temperature rise is limited, because they assumed that the laser absorption by plasma is independent of temperature.

Heat accumulation effect has been analyzed using more precise thermal conduction model that can simulate laser absorption region as well as the melt dimensions at high pulse repetition rates by Miyamoto *et al* [15,16]. Their paper indicates that the laser absorption region extends toward the laser source up to the region where the laser intensity is much lower than multiphton ionization threshold at high pulse repetition rates. This suggests thermally ionized electrons contribute as seed electrons for avalanche ionization to ionize without multiphoton ionization in the extended region. In this situation, plasma shielding effect near the geometrical focus is expected to be significant, since more laser energy is consumed upstream.

In experimental approach, new findings have been reported by several authors through the observation of plasma behavior using high-speed video camera without lighting [17] and a pump-probe technique [18]; the observation shows that small plasma with a size of focus volume does not stay at a fixed position but moves upwards periodically to cover the region much larger than focus volume. While plasma motion is speculated to be gaseous volume driven by buoyancy in [18], the observed plasma motion seems to be too fast to attribute to buoyancy.

In the present paper, ionization process is simulated with taking into consideration the effects of heat accumulation effect that provides thermally ionized electrons for seeding avalanche ionization and plasma shielding as well to account for the dynamic plasma motion observed at high pulse repetition rates [17].

## 2. Observation of laser-matter interaction

*fs*-laser pulses (IMRA; pulse duration $\tau_p = 550\ fs$, wavelength $\lambda = 1045\ nm$) is focused into borosilicate glass plate (D263, Schott) using NA0.65 lens at a depth of approximately 250 $\mu m$ from the surface of the glass sample (thickness 1 *mm*). Side-polished glass plate are irradiated by *fs*-laser pulses in perpendicular to the plate thickness. Photographs are taken from the side with high-speed video camera (Photron Fastcam) at a frame rate of 50,000 *kHz* and an exposure time of 5.4 $\mu s$ without auxiliary lighting. When the *fs*-laser pulses are irradiated at a pulse repetition rate of 1 *MHz*, for instance, pictures are taken at each 20 pulses with overlapped images of 5 ~ 6 pulses. While the filming rate is not high enough to observe the plasma evolution pulse-by-pulse, dynamic behavior of the plasma in longer time scale, which has never observed in the past, can be observed. The cross-section and side view of the laser-irradiated glass samples are observed by an optical microscope.

**Figures 1(a)** and **(b)** show a cross-section and a side view of the laser-irradiated glass sample obtained at pulse repetition rate $f = 1$ MHz, pulse energy $Q = 2.5\ \mu J$ and translation speed $v = 20\ mm/s$. The cross-section shows a dual-structure [15] consisting of a teardrop-shaped inner structure and an elliptical outer structure. Our thermal conduction model [5,15,16] indicates that the laser energy is absorbed in the inner structure, and that the glass is melted in the outer structure where working point with a viscosity $10^4\ dPas$ (1,050 $^\circ C$) is reached. The dual-structure is also clearly observed in the side view (Fig. 1b). The vertical size of the inner structure changes at some distance from the beginning, which corresponds to several thousands of laser pulses.

**Figure 1(c)** shows a snap shot of the laser-induced plasma in moving glass sample due to USLPs at 1 *MHz* impinged. As will be described below we found that small plasma moves within the region of the inner structure where the laser energy is absorbed [15]. It is noted that the plasma size is as small as the focus volume, which is much smaller than that of the inner structure. This suggests the plasma temperature is locally much higher than the value simulated based on thermal conduction model [15] and rate equation model [13] assuming the plasma fills the inner structure.

**Figure 2** shows a series of high-speed pictures taken under the same condition as Fig.1. The high-speed pictures reveal striking fact that the plasma evolution is localized in the small part of the inner structure, and shows cyclic change in height, dimensions, and brightness. The cyclic plasma evolution is characterized by semi-cyclic behavior consisting of generation of plasma near the focus (#2), upward expansion (#3~#24) and disappearance at the highest position (#26~#31). It is noted that long and thin linear plasma produced near the focus expands upward rapidly (#2 and #6) during a plasma spot in the previous cycle still exists at the highest

position. Then the expansion speed is slowed down gradually with changing its shape from linear to sphere; sometimes it breaks down into two smaller pieces. At maximum height, the plasma decreases its brightness and the size, and disappears eventually. It is interesting to note that the plasma is produced when the plasma with less brightness still exists, and two plasmas coexist at different heights as seen in #2~#7. This suggests that the upper plasma is partially transparent.

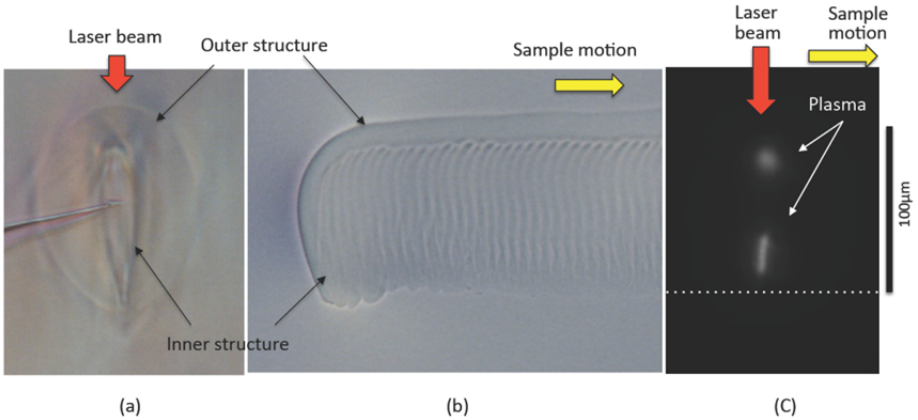


Fig. 1. (a) Cross-section of internal modification. The sample moves perpendicularly to the paper plane. (b) Side-view of the modified glass sample. Vertical sizes of inner and outer structure vary at the beginning of approximately 100 $\mu m$. (c) A snapshot of laser-induced plasma taken from side. The location of geometrical focus is shown by a dotted line. ($f$ = 1 $MHz$, Q = 2.5 $\mu J$, $v$ = 20 $mm/s$).

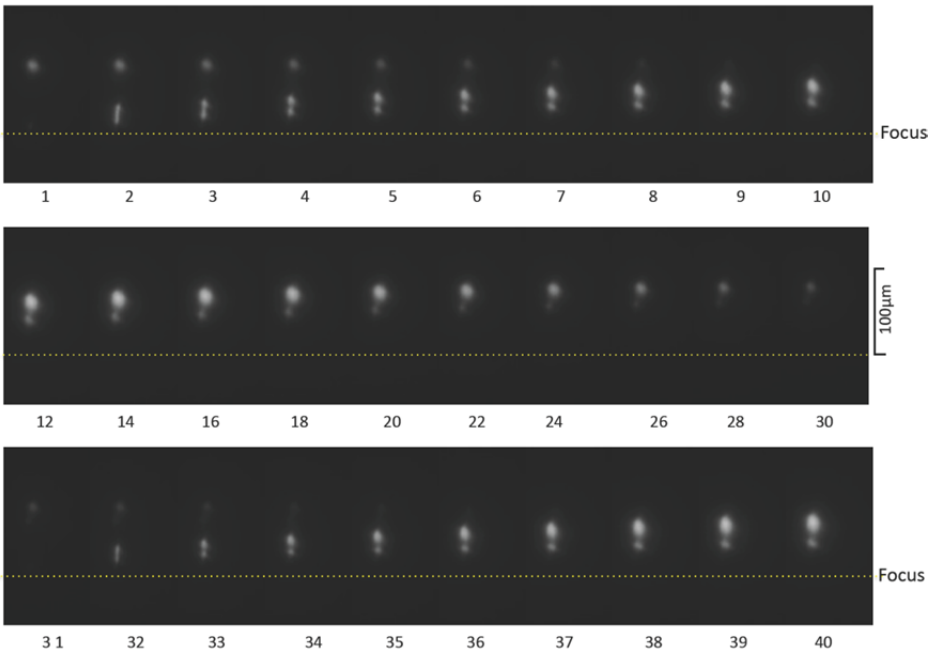


Fig. 2. High-speed pictures taken at a frame rate of 50,000 per second under conditions of $f$ =1$MHz$, $Q$ = 2.5 $\mu J$, $v$ = 20 $mm/s$ in D263. Figures indicate the relative number of the frame.

**Figure 3** shows the change in the height of the plasma at its top and bottom with respect to the geometrical focus from the first laser pulse. It is noted that the frequency of the cyclic plasma evolution is approximately two orders smaller than the repetition rate of the *fs*-laser pulses. Change of the maximum height and cycle of the plasma evolution is clearly observed. The figure also shows steady height of the inner and outer structure are reached after 3,000~4,000 pulses in $f$ = 1 $MHz$ condition, in accordance with the variation of vertical size of the inner structure shown in Fig. 1(b).

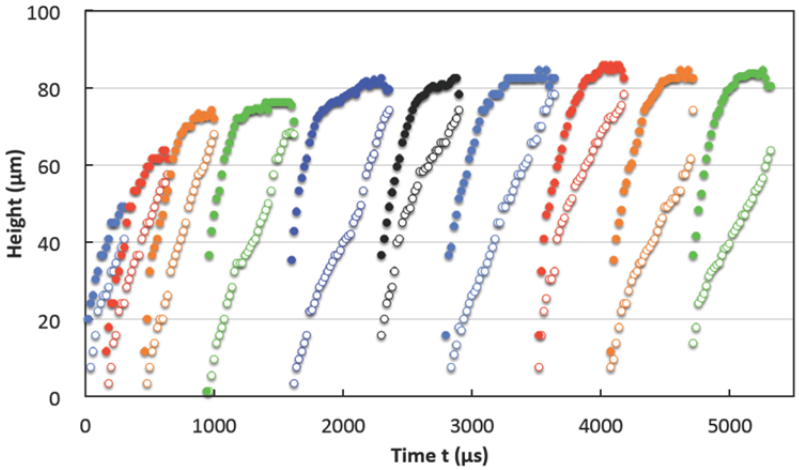


Fig. 3. Vertical position of the plasma at its top and bottom with respect to the geometrical focus is shown by closed and open circles, respectively, plotted from the first laser pulse (f=1*MHz*, Q=2.5 *μJ* and v=20 *mm/s*, D263).

## 3. Analysis of laser-matter interaction based on numerical simulation

### *3.1. Simulation model*

Temporal evolution of free-electron density $\rho(z,t)$ in internal modification by USLPs is given by the following rate equation [11-13]

$$\frac{\partial \rho(z,t)}{\partial t} = \eta_{photo} I^K(z,t) + \eta_{casc}\rho(z,t) - \eta_{rec}\rho(z,t)^2 \tag{1}$$

where $\eta_{photo}$ is photo ionization coefficient, $\eta_{casc}$ avalanche ionization coefficient, $\eta_{rec}$ recombination coefficient and $K$ number of photon for photoionization, which is given by the integer part of $(E_g/\hbar\omega+1)$. The avalanche ionization coefficient $\eta_{casc}$ is given by [11]

$$\eta_{casc} = \frac{1}{\omega_L^2\tau^2+1}\left[\frac{e^2\tau}{cn_0\varepsilon_0 m(3/2)E_g} I(z,t) - \frac{m\omega_L^2\tau}{M}\right] \tag{2}$$

where $\tau$ is time between collision for inverse Bremsstrahlung, $c$ light speed in vacuum, $n_0$ refractive index of the medium at laser-frequency $\omega_L$, $m$ electron mass, $M$ molecular mass, $\varepsilon_0$ vacuum permittivity, and $E_g$ effective ionization potential. In this study, self-focusing and refraction of laser beam in plasma are neglected as the first step. Then the laser intensity in transparent dielectrics is given by

$$I(z,t) = \frac{2Q}{\tau_p \pi \omega(z)^2}\exp\left[-4\ln 2\left(\frac{t - n_0(z-z_f)/c - 2\tau_p}{\tau_p}\right)^2 - \int_0^z \alpha(z,t)\,dz\right] \tag{3}$$

where $Q$ is laser pulse energy, $z_f$ focus position and $\tau_p$ pulse duration. $\omega(z)$ is laser spot radius given by

$$\omega(z) = \omega_0\sqrt{1+\left(\frac{z-z_f}{z_R}\right)^2}, \tag{4}$$

where $z_R$ is Rayleigh length and $\omega_0$ laser spot radius at waist. Then the absorption coefficient $\alpha(z,t)$ is given by

$$\alpha(z,t)I(z,t) = \eta_{photo} I^K(z,t) + \eta_{casc} I(z,t)\rho(z,t) \tag{5}$$

In internal modification by USLPs at high pulse repetition rates, thermally ionized electrons play an important role for seeding avalanche ionization in addition to photoionization, since laser beam is incident to the material with high temperature due to heat accumulation effect. When USLPs with Gaussian distribution and $z$-intensity

distribution q(z') are absorbed in an infinite body moving at a constant speed of $v$ along $x$ axis, the temperature rise at time $t$ is given by

$$T(x,y,z,t)=\frac{1}{\pi c_g \rho_g}\sum_{i=1}^{n}\frac{1}{\sqrt{\pi k\{t-(i-1)/f\}}}\int_{-\infty}^{\infty}\frac{q(z')}{\omega^2(z')+8k\{t-(i-1)/f\}}\exp\left[-\frac{2\left\{\left(x+v\{t-(i-1)/f\}\right)^2+y^2\right\}}{\omega^2(z')+8k\{t-(i-1)/f\}}-\frac{(z-z')^2}{4k\{t-(i-1)/f\}}\right]dz'. \quad (6)$$

where $c_g$ is heat capacity, $\rho_g$ density, $k$ thermal diffusivity and $f$ pulse repetition rate. The thermally ionized electron density at elevated temperature is calculated by Saha equation. In this simulation, radiation loss and dependence of thermal properties on temperature are neglected for simplicity. Within the condition tested in this study, multi-photon ionization (MPI) dominates rather than tunneling ionization in the photoionization process, since Keldysh parameter $\gamma$ [19] is significantly larger than 1 due to decrease in laser intensity near the focus by plasma shielding effect as will be described below. For $\eta_{photo}$, we used Kennedy's approximation [12] of the Keldysh model [19].

### *3.2. Laser-matter interaction*

**Figure 4** shows the distribution of free-electron density $\rho_{JAP}$ (just after pulse), laser intensity in glass during interaction $I_P$ and laser transmission $L_{trans}$, when $Q$ = 2.5 $\mu m$ is incident to the glass sample with a geometrical focus at a position of $z_f$ = 250 $\mu m$ from the surface. In the figure, laser intensity without laser absorption $I_0$ is also plotted by a solid line. It is seen the peak locations of $I_P$ and $\rho_{JAP}$ are shifted upstream toward the laser source from the geometrical focus $z_f$ by approximately 20 ~ 30 $\mu m$. This is because the laser energy is consumed in the upper stream by multiphoton and avalanche ionizations, and thereby the material near the focus is shielded by thus created plasma. The peak laser intensity actually interacting with the plasma is reduced down to the value nearly one order smaller than incident laser beam, which provides Keldysh parameter large enough to use multiphoton ionization approximation.

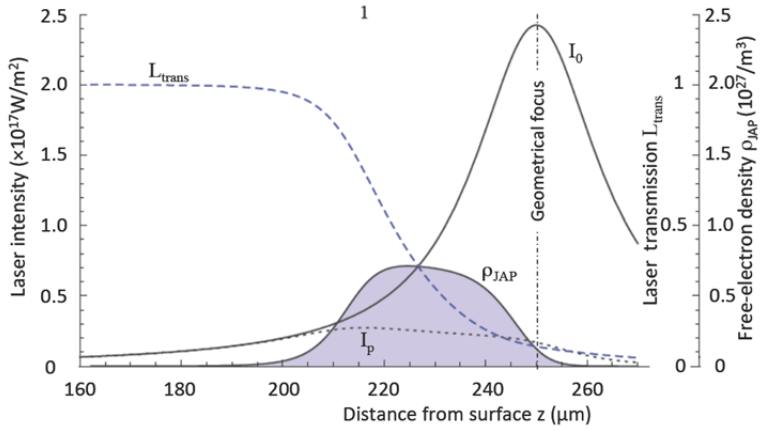


Fig. 4. Distribution of free-electron density $\rho_{JAP}$ just after first laser pulse. Laser intensity ($I_p$: in plasma, $I_0$: without absorption) and transmission of laser energy $L_{trans}$ are also plotted vs. $z$. Laser beam propagates from left to right to focus at $z_f$ = 250 $\mu m$ ($Q$ = 2.5 $\mu J$, $z_R$ = 15 $\mu m$).

**Figure 5** shows the temperature variation simulated at $z$ = 240 $\mu m$, for instance, when five pulses impinge at a pulse repetition rate of 1 *MHz*. The temperature rises stepwise at the moment of the pulse impingement, and then cooled down by thermal diffusion between the laser pulses to the peripheral low temperature region. In the figure, temperatures just before and after 4$^{th}$ laser pulse, for instance, are shown by $T_{JBP}$ and $T_{JAP}$, respectively. The 4$^{th}$ laser pulse interacts with material at temperature $T_{JBP}$ under the influence of free-electron density of $\rho_{JBP}$ to provide $T_{JAP}$.

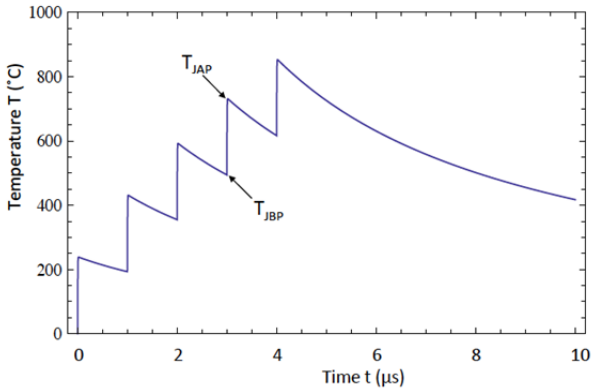


Fig. 5. Temperature variation simulated at $z = 240\ \mu m$ ($Q = 2.5\ \mu J$ and $f = 1\ MHz$). In the figure, temperature just before and after 4th laser pulse are shown by $T_{JBP}$ and $T_{JAP}$, respectively.

The temperature distributions $T_{JBP}$ are simulated without and with the effect of thermally ionized electrons, and are plotted in **Figs. 6(a)** and **(b)**, respectively. In the former case, while heat is accumulated by a series of laser pulses, the same laser energy distribution is absorbed repeatedly. Then the temperature rises monotonically due to simple heat accumulation producing similar curves, and tend to saturate with increasing pulse number, as seen in Fig. 6(a).

In the later case, laser absorption is affected by thermally ionized electrons. Then the temperature curves are affected not only by heat accumulation but by the thermally ionized electrons, which contribute as the seed electrons for avalanche ionization. It is seen the temperature distribution in the later case is basically the same as the former case up to pulse number of $n \approx 12$. However, the temperature distribution curves become completely different from the former case in $n > 12$; the peak of each curve is elevated to higher temperature and the peak position begins to move toward the laser source. After reaching highest value at $n \approx 33$, the peak value and moving speed tend to decrease. In the decreasing phase ($n > 33$), the second peak appears near the geometrical focus (end of first cycle). The second peak is elevated in accordance with the decrease of the first peak value (beginning second cycle). In the second cycle, the peak temperature exceeds the values of the first cycle. Such a dynamic motion of the temperature filed is qualitatively in accordance with the experimental observation of plasma described in section **2**. As the cycle number increases, peak temperature and the shift of the curve toward upstream tend to increase, until steady state is reached at several tens cycles.

Dotted line shows T = 3,600 ˚C, which corresponds to the temperature at the contour of the laser absorption region estimated by the thermal conduction model [15,16]. It is interesting to note that the wider region is exposed to the temperature T > 3,600 ˚C than the case of the simple heat accumulation model [14] despite the fact that transient temperature distribution is concentrated to narrower region, when the contribution of thermally ionized electron is taken into account.

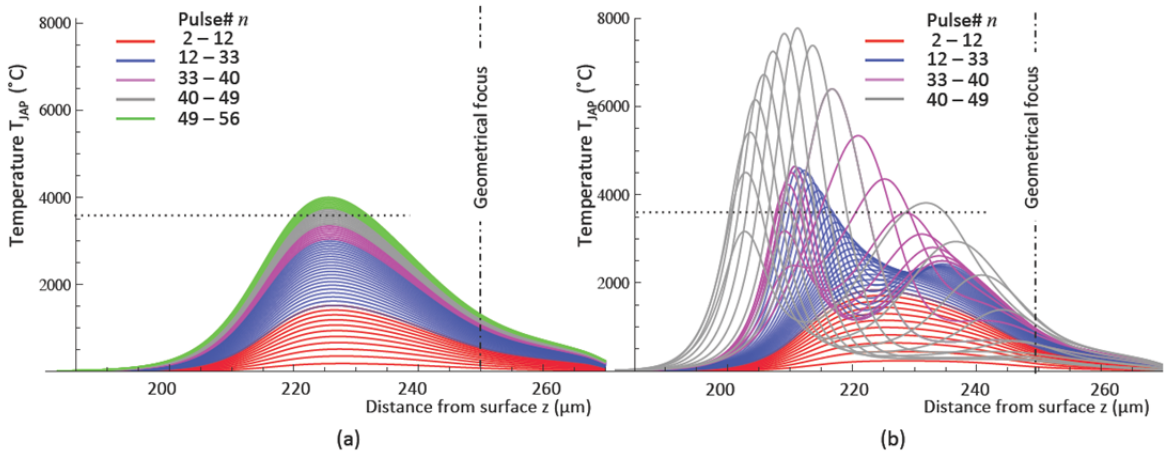


Fig. 6. Distribution of $T_{JBP}$ along $z$-axis at different pulse numbers simulated (a) without and (b) with the effect of thermally ionized electrons at different pulse numbers. Dotted line shows T = 3,600 ˚C, which corresponds to the laser absorption region [15,16].

### *3.3. Interaction at high pulse repetition rates*

In order to understand the mechanism behind the dynamic plasma motion shown by temperature variation in Fig. 6(b), free-electron density simulated just before ($\rho_{JBP}$) and after laser pulse ($\rho_{JAP}$) are plotted along with laser transmission $L_{trans}$ and temperature rise $T_{JBP}$ at different pulse numbers of $n$ = 39 ~ 49 in **Fig. 7**. In the figure, increase of free-electron density $\Delta\rho = \rho_{JBP} - \rho_{JAP}$ is plotted by a dashed red line.

In $n$ = 39 ~ 43 where the plasma is exposed to high intensity laser beam, large absorption coefficient α is reached by the appreciable amount of thermally ionized electron density $\rho_{JBP}$ providing larger $\Delta\rho$. Thus the laser absorption concentrates to the narrow region with a size of approximately 10 $\mu m$ at the location some distance ahead the plasma, allowing the small plasma to move toward the laser source.

In $n$ = 45 ~ 49 where the laser intensity is decreased due to the movement of the plasma toward the laser source, the laser energy is absorbed rather uniformly due to the reduction of the absorption coefficient $\alpha$, so that the forward plasma motion is slowed down due to the reduction of $\Delta\rho$. The reduction of $\alpha$ also makes the plasma less opaque, so that a new plasma is produced by the transmitted laser energy through the plasma by MPI near the geometrical focus.

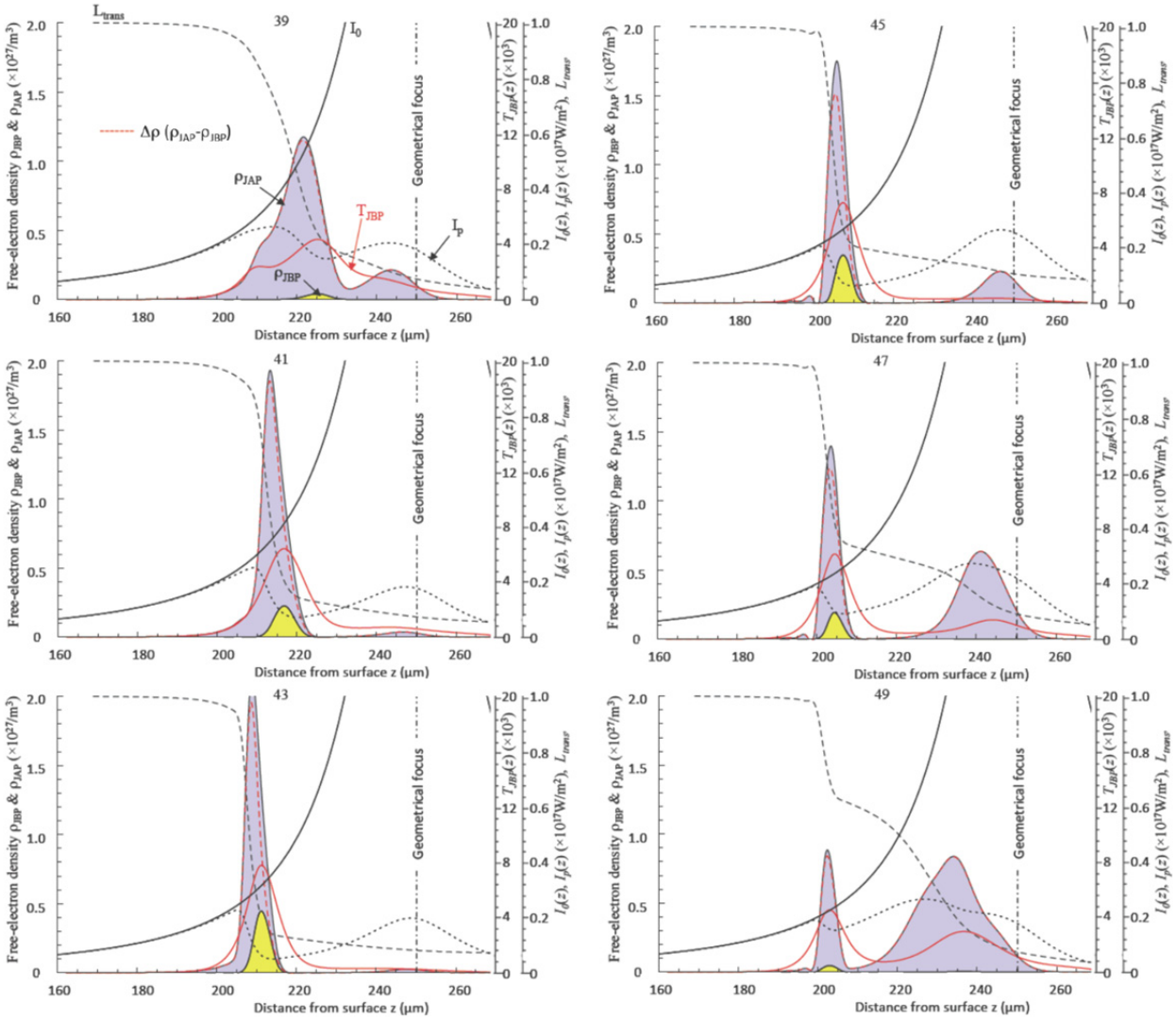


Fig. 7. Distribution of free-electron density ($\rho_{JBP}$ & $\rho_{JAP}$), temperature rise $T_{JAP}$ just after laser pulse at different pulse numbers. Laser intisity ($I_p$: with plasma, $I_0$: without plasma) and transmission of laser energy $L_{trans}$ are plotted vs. $z$. Laser beam propagates from left to right to focus at $z_f = 250\ \mu m$. Dashed red line shows increase of free-electron density given by $\Delta\rho$ ($=\rho_{JAP} - \rho_{JBP}$) in single laser pulse.

In **Fig. 8**, the peak positions of temperature $T_{JBP}$ and free-electrons $\rho_{JBP}$ just before the impingement of the laser pulse are plotted vs. number of laser pulses. It is seen that almost perfect agreement is observed between two curves, supporting our model that the dynamic plasma motion is caused basically by the thermally ionized electrons at high pulse repetition rates. The figure also shows the extent of the plasma motion shifts increasingly toward the laser source as the cycle number increases, in agreement with the experimental observation shown in Fig. 3.

Interestingly some fluctuation of the peak location is found in the geometrical focus side, while no systematic variation exists in the extent of the geometrical focus side. This suggests that some nondeterministic process is included, despite that the ionization process near the focus is basically governed by MPI, which should be deterministic. This is considered to be because the laser intensity near the geometrical focus is strongly affected by the laser absorption in the plasma, which depends on the temperature distribution of the plasma.

It should be noted, however, that the plasma motion simulated by our model provides significantly shorter repeating cycle than the experimental observation shown in Fig. 3, and simulated electron density and temperature seem to be overestimated. Nevertheless our model can explain the dynamic plasma motion at high pulse repetition rates qualitatively. Further improvement of the model is needed.

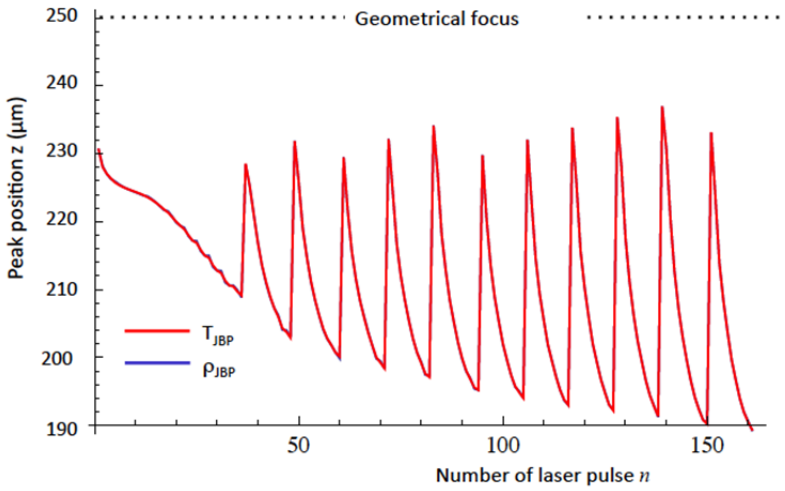


Fig. 8. Location of maximum temperature $T_{JBP}$ and free-electron density $\rho_{JBP}$. Laser beam incident from the bottom of the picture. Two curves are in agreement almost perfectly, indicating the dynamic plasma motion is caused by thermal electrons.

## 4. Concluding remarks

We previously reported dynamic plasma motion using high-speed video camera showing unexpected dynamic behavior that high brightness plasma moves semi-periodically toward the laser source within laser-absorption region when *fs*-laser pulses at 1 *MHz* is irradiated into borosilicate glass. In order to explain the experimental observation, temporal evolution of free-electrons and temperature due to USLPs at high pulse repetition rates in transparent dielectrics are simulated based on rate equation model of free-electrons and thermal conduction model with taking into consideration the plasma shielding effect. The simulation shows that thermally ionized electrons play an important role in ionization process to provide the semi-periodic plasma motion by contributing as the seed electrons for avalanche ionization in qualitatively accordance with our previous experimental observation. It is shown that the ionized region expands much longer distance toward the laser source where mulitiphoton ionization threshold is not reached than the case of single pulse irradiation, while the ionization region near the focus is nearly fixed.

## Acknowledgements

This work was partially supported by Erlangen Graduate School in Advanced Optical Technologies (SAOT).

## References

[1] K.M. Davis, K. Miura, N. Sugimoto, and K. Hirao, “Writing waveguides in glass with a femtosecond laser,” Opt. Lett., **21** 1729-1731 (1996).
[2] C. Miese, M. J. Withford, A. Fuerbach, “Femtosecond laser direct-writing of waveguide Bragg gratings in a quasi cumulative heating regime”, Opt. Express, 19, 19542-19550 (2019)
[3] A. Arriola, S. Gross, N. Jovanovic, N. Charles, P. G. Tuthill, S. M. Olaizola, A. Fuerbach, M. J. Withford: “Low bend loss waveguides enable compact, efficient 3D photonic chips”, Opt. Express, **21**, 2978 - 2986 (2013).
[4] T. Tamaki, W. Watanabe, J. Nishii, and K. Itoh, “Welding of transparent materials using femtosecond laser pulses,” Jpn. J. Appl. Phys. **44**, L687–L689 (2005).
[5] I. Miyamoto, K. Cvecek, M. Schmidt, “Characteristics of laser absorption and welding in FOTURAN glass by ultrashort laser pulses”, Optics Express, **19**, 22961-22973 (2011).
[6] S. Richter, S. Döring, A. Tünnermann and S. Nolte, “Bonding of glass with femtosecond laser pulses at high repetition rates,” Appl. Phys. A: Materials Science & Processing **103**, 257–261 (2011).
[7] C. Hnatovsky, R.S. Taylor, E. Simova, P.P.Rajeev, D.M. Rayner, V.R. Bhardwaj, P.B. Corkum, “Fabrication of microchannels in glass using focused femtosecond laser radiation and selective chemical etching”, Appl. Phys. A **84**. 47-61 (2006).
[8] D. Wortmann, J. Gottmann, N. Brandt, H. Horn-Solle: “Micro- and nanostructures inside sapphire by fs-laser irradiation and selective etching”, Opt. Express, 16 (2008) 1517-1522
[9] Y. R. Shen: “Principle of nonlinear optics”, NewYork: Wiley (1984) 528-539
[10] Stuart, M.D. Feit, S. Herman, A.M. Rubenchik, B.W. Shore, and M.D. Perry, “Nanosecond-to-femtosecond laser-induced breakdown in dielectrics,” Phys. Rev. B **53**, 1749-1761 (1996).
[11] A. Vogel, J. Novak, G. Hüttman, and G. Paltauf, “Mechanisms of femtosecond laser nanosurgery of cells and tissues,” Appl. Phys. B **81**(8), 1015–1047 (2005).
[12] P. K. Kennedy, “A first-order model for computation of laser-induced breakdown thresholds in ocular and aqueous media: Part I – Theory,” IEEE J. Quant. Elect., **31** 2241-2249 (1995).

[13] M. Sun, U. Eppelt, W. Schulz, J. Zhu: Role of thermal ionization in internal modification of bulk borosilicate glass with picosecond laser pulses at high repetition rates, Opt. Mat. Express **3,** 1716 (2013).

[14] Schaffer, J.F. Garcia, E. Mazur, "Bulk heating of transparent materials using high-repetition-rate femtosecond laser," Appl.. Phys. A 76, 187-208 (2003).

[15] I. Miyamoto, K. Cvecek, M. Schmidt, "Evaluation of nonlinear absorptivity in internal modification of bulk glass by ultrashort laser pulses", Opt. Express, **19**, 10714-10727 (2011).

[16] I. Miyamoto, K. Cvecek, Y. Okamoto, M. Schmidt: "Internal modification of glass by ultrashort laser pulse and its application to microwelding", Appl. Phys. A (2014) 114, 187–208

[17] I. Miyamoto, Y. Okamoto, R. Tanabe, Y. Ito: "Characterization of plasma in microwelding of glass using ultrashort laser pulse at high pulse repetition rates", Proc. 8th LANE (2014)

[18] I. Alexeev , J.Heberle , K. Cvecek , K.Yu. Nagulin, M. Schmidt, High speed pump-probe apparatus for observation of transitional effects in ultrafast laser micromachining processes, *Micromach.* 2015, *6* (12), 1914-1922.

[19] L. V. Keldysh: "Ionization in the field of a strong electromagnetic wave", Sov. Phys. JETP (1965) 1207-1314.